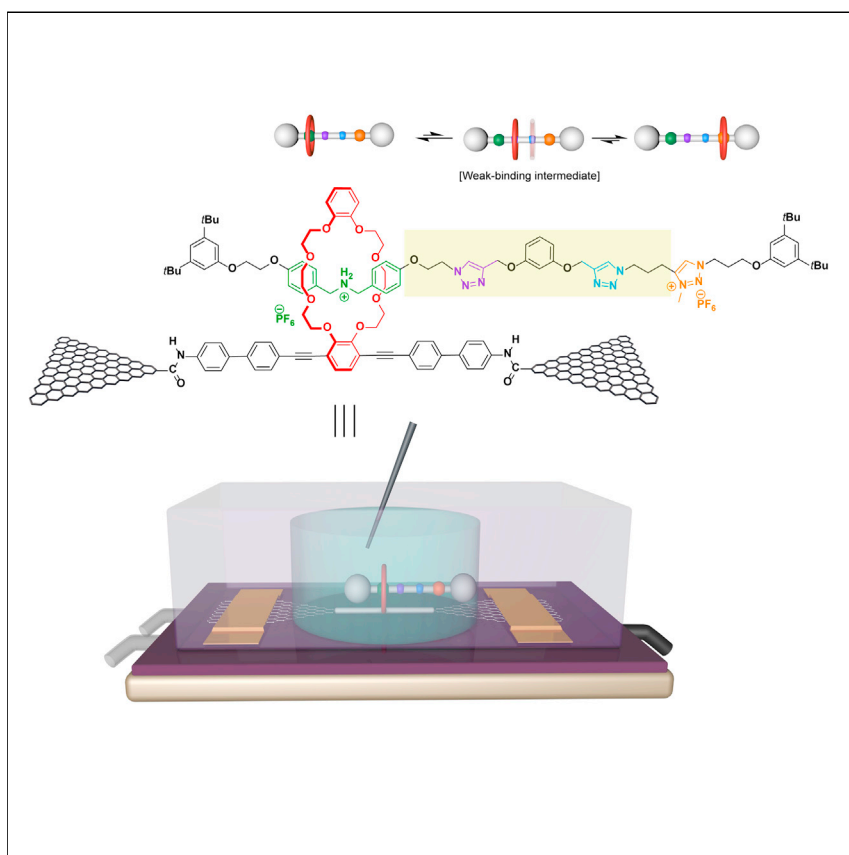


Article

Real-time observation of the dynamics of an individual rotaxane molecular shuttle using a single-molecule junction



Real-time graphene-molecule-graphene single-molecule junction (GMG-SMJ) measurements on an individual [2]rotaxane molecule reveal shuttling dynamics, including a previously unidentified weak-binding intermediate, providing an opportunity to elucidate the dynamics of synthetic molecular machines hidden by techniques that report the averaged behavior of an ensemble.

Sujun Chen, Dingkai Su,
Chuancheng Jia, ..., Xuefeng
Guo, David A. Leigh, Liang
Zhang

guoxf@pku.edu.cn (X.G.)
david.leigh@manchester.ac.uk (D.A.L.)
zhangliang@chem.ecnu.edu.cn (L.Z.)

Highlights

Real-time measurements of
kinetics and thermodynamics of a
single molecular shuttle

Formation of a short-lived weak-
binding intermediate is directly
observed

Single-molecule junctions show
aspects hidden to methods that
report averaged behavior

Article

Real-time observation of the dynamics of an individual rotaxane molecular shuttle using a single-molecule junction

Sujun Chen,^{1,8} Dingkai Su,^{2,8} Chuancheng Jia,⁴ Yanwei Li,^{5,6} Xingxing Li,⁷ Xuefeng Guo,^{2,4,*} David A. Leigh,^{1,3,*} and Liang Zhang^{1,9,*}

SUMMARY

Measurements on single molecules can sometimes reveal features that can be difficult to detect using techniques that probe the averaged properties of many molecules. Here, we report on the use of graphene-molecule-graphene single-molecule junctions (GMG-SMJs) to probe the shuttling dynamics of an individual [2]rotaxane molecule. The experiments show variations in the thermodynamic and kinetic shuttling parameters over a temperature range, and in different solvents, allowing the single-molecule data to be quantitatively related to simulation and ensemble experiments. The structural (~1 nm) and temporal (~17 μ s) resolution of the GMG-SMJ enables direct observation of a previously unidentified weak-binding intermediate, arising from the formation of weak hydrogen bonds between the ring and triazole units. The results illustrate how GMG-SMJ measurements provide new opportunities for elucidating aspects of the structure, dynamics, and operational mechanisms of synthetic molecular machines that may be hidden to techniques that probe averaged behavior of an ensemble.

INTRODUCTION

Rotaxane-based molecular shuttles, molecules featuring a macrocycle threaded onto a molecular axle,¹ are prototypical artificial nanomachines that undergo well-defined, large amplitude, dynamics of one mechanically interlocked component with respect to the other.^{2–8} The exchange of the ring between different positions on the thread is mediated by the relative interaction strengths of the ring with various sites on the axle. The dynamics of molecular shuttles has generally been studied in solution, using a range of techniques that interrogate the average behavior of many molecules, such as NMR, IR, and electrochemistry.^{9–16} Although most rotaxanes are far smaller than typical motor proteins, the first accounts of the use of single-molecule force spectroscopies^{17–24} (SMFS) and optical tweezers²⁵ to probe such systems have been described. Nevertheless, the real-time measurement of the kinetics and thermodynamics of individual molecular shuttles, particularly temperature-dependent behavior that can be hard to obtain using single-molecule force spectroscopy, remains a significant technical and scientific challenge.

Graphene-molecule-graphene single-molecule junctions²⁶ (GMG-SMJs) are simple to fabricate, low cost, label free, and offer an alternative means of obtaining real-time measurements on the structural dynamics of single molecules. They have previously been used to probe host-guest complexation,^{27–29} single-molecule chemical reactions,^{30–33} and hydrogen-bonding dynamics.³⁴ Incorporating molecular

The bigger picture

Understanding dynamics is indispensable for designing machines at all length scales. Motor protein dynamics are often studied using single-molecule techniques. In contrast, artificial nanomachines, being substantially smaller than biomolecular machines, are generally studied in bulk solutions using tools that measure the averaged behavior of many molecules. Here, we probe the temperature- and solvent-dependent shuttling dynamics of individual rotaxane molecules using graphene-molecule-graphene single-molecule junctions (GMG-SMJs). The results include direct observation of a short-lived intermediate state in the single-molecule studies that is not revealed by spectroscopies that measure ensemble averaged dynamics. Tools and methods that probe the structure and dynamics of single molecules, such as SMJ experiments, can play an important role in molecular machine design through the discovery of states and (co-) conformations that are not revealed by techniques that report on averaged behavior.



machinery into GMG-SMJs provides an opportunity to directly observe the structure and dynamics of complex nanoscale architectures, as well as help establish functional circuits that can respond to and interact with molecular-level events.^{35,36} Accordingly, we investigated the temperature- and solvent dependence of the shuttling motion of the ring in a hydrogen bonded rotaxane using a graphene-molecule-graphene single-molecule junction.

RESULTS AND DISCUSSION

Molecular design and single-molecule device fabrication

The [2]rotaxane-based molecular shuttle **1** is based on the well-established^{37–48} crown-ether-dibenzylammonium-triazolium system. The axle was designed to have two principal binding sites for the crown ether, namely, a dibenzylammonium motif (DBA) and a methyl triazolium group (MTA). These two sites are positioned at either end of a ~4 nm axle, which also features two triazole units (TA1 and TA2) used to assemble the complete axle through copper-catalyzed azide-alkyne cycloaddition (CuAAC) “click” reactions. The DBA unit has a higher binding affinity for the dibenzo-24-crown-8 (DB24C8) crown ether than the MTA group, which should generate unequal lifetimes for the two dynamically exchanging co-conformers, *DBA-1-SMJ* and *MTA-1-SMJ* (the italicized prefixes denote the position of the ring in the different co-conformers). Bulky 3,5-di-*tert*-butylbenzyl groups terminate the axle ends to prevent dethreading. In order to bridge the nanogapped graphene point contacts, a rigid conjugated organic strut with two amine handles was incorporated into the dibenzo[24]crown-8 unit, **2**. The formation of [2]rotaxane **1**, followed by covalent attachment to the carboxylate groups on the edges of graphene sheets by an 1-ethyl-3-(3-dimethylaminopropyl)carbodiimide-mediated condensation reaction, generated the single-molecule functional unit **1-SMJ** (Figure 1A; Sections S3 and S4).

The formation of the GMG-SMJs was verified by measuring the current-voltage relation (*I*-*V*) curves of the devices. Under low voltage bias, a typical molecular *I*-*V* curve was detected (*I*_D recovered to some extent) (Figure 1B). By optimizing the exposure parameters and etching conditions, the connection yield was raised to ~16%; that is, 20 of the 126 devices on the same substrate showed recovery of conductance. The statistical analysis results based on the binomial distribution suggested the probability of forming each single-molecule connection is ~92% (Section S5), confirming that the charge transport through the junction was mainly sustained by **1-SMJ**. Moreover, all of the working devices exhibited similar electrical properties in the subsequent shuttling experiments, demonstrating good reproducibility of the SMJ structure and process (Section S6.1).

Real-time electrical measurement

Using a specific temperature control module and a polydimethylsiloxane (PDMS) solvent reservoir (Figure 1C), real-time monitoring of the shuttling behavior of **1-SMJ** was performed at the graphene-liquid interface. Time-dependent electrical characterization was carried out at a high-speed sampling frequency with the **1-SMJ**s immersed in acetonitrile (CH₃CN) at 298 K. Unlike the ¹H NMR spectrum of **1** (500 MHz, CD₃CN, 298 K; Section S3), which shows shifts principally to the DBA signals sites, as that is the axle region encapsulated by the ring in the major co-conformer (*DBA-1-SMJ*), the current-time (*I*-*t*) curve of **1-SMJ** shows fluctuations from the major co-conformer to another relatively short-lived state (Figure 2A). The resulting current-count histogram shows a bimodal distribution centered at 32 and 69 nA (Figure 2B), respectively. This is consistent with the second state being the DB24C8 ring transiently located on the weaker binding MTA site, i.e., *MTA-1-SMJ*.

¹School of Chemistry and Molecular Engineering, East China Normal University, Shanghai 200062, P.R. China

²State Key Laboratory for Structural Chemistry of Unstable and Stable Species, Beijing National Laboratory for Molecular Sciences, National Biomedical Imaging Center, College of Chemistry and Molecular Engineering, Peking University, Beijing 100871, P.R. China

³Department of Chemistry, University of Manchester, Oxford Road, Manchester M13 9PL, UK

⁴Center of Single-Molecule Sciences, Frontiers Science Center for New Organic Matter, Tianjin Key Laboratory of Micro-Scale Optical Information Science and Technology, Institute of Modern Optics, College of Electronic Information and Optical Engineering, Nankai University, 38 Tongyan Road, Jinnan District, Tianjin 300350, P.R. China

⁵Shenzhen Research Institute, Shandong University, Shenzhen 518057, P.R. China

⁶Environment Research Institute, Shandong University, Qingdao 266237, P.R. China

⁷Hefei National Laboratory for Physics Sciences at the Microscale, University of Science and Technology of China, Hefei, Anhui 230026, P.R. China

⁸These authors contributed equally

⁹Lead contact

*Correspondence: guoxf@pku.edu.cn (X.G.), david.leigh@manchester.ac.uk (D.A.L.), zhangliang@chem.ecnu.edu.cn (L.Z.)

<https://doi.org/10.1016/j.chempr.2021.11.012>

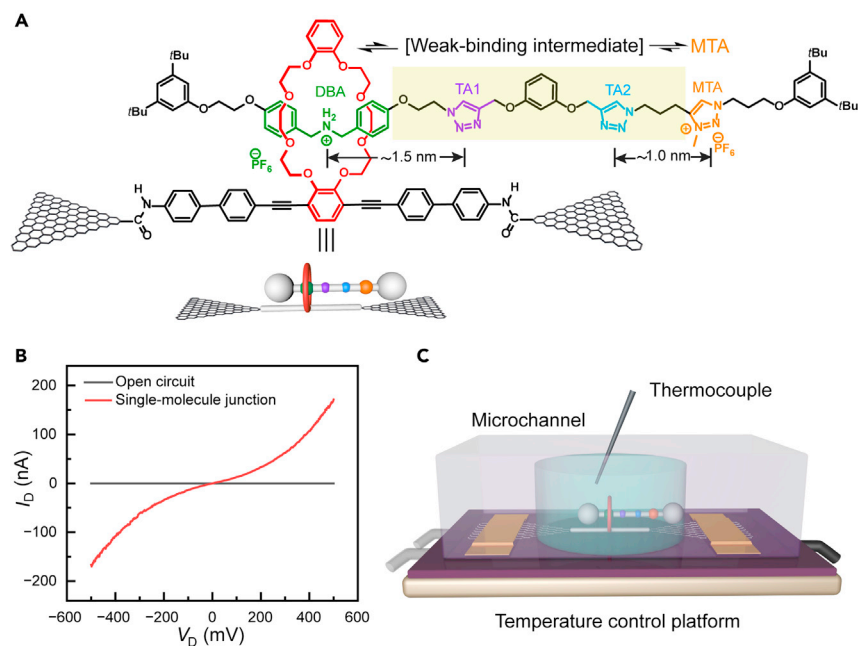


Figure 1. Fabrication and electronic characterization of 1-SMJ devices

(A) Chemical structure of 1-SMJ. Molecular shuttle 1 contains DBA and MTA units as the principal binding sites, bridged by a spacer containing two triazole rings (TA1 and TA2) and a 1,3-phenyl diether group. The distance between DBA and TA1 is ~ 1.5 nm; the distance between MTA and TA2 is ~ 1.0 nm.

(B) Current-voltage (I - V) curves of graphene contacts (black) and 1-SMJ (red) in the solid state. The black curve shows that no current occurs after etching. The current (red) through a 1-SMJ device indicates a successful single-molecule connection.

(C) Schematic representation of 1-SMJ device-liquid interface characterization platform. The 1-SMJs were fixed on a precise temperature controlled platform and covered with a polydimethylsiloxane reservoir.

To rule out artifacts, a control experiment was performed by forming an GMG-SMJ using only the ring component, 2. The resulting I - t curve and current-count histograms for 2-SMJ showed a single conductance level (Section S6.2), rather than a bimodal distribution, excluding the possibility of the conjugated backbone being the source of the electrical spikes observed with 1-SMJ.

To obtain a better understanding of the correlation between the current flip-flops and the shuttling process in 1-SMJ, the transmission spectra of GMG-SMJs with the DB24C8 located at DBA, MTA, TA1, and TA2 were calculated using an equilibrium Green's function technique based on density functional theory (DFT), as implemented in the Atomistix ToolKit (ATK) package (Section S8). The molecular geometries were optimized at M06-2X/6-31G(d) level, whereas the single-point energy calculations were conducted at M06-2X/6-311+G(d,p) level with a solvation model based on density (SMD) in both acetonitrile and dimethyl sulfoxide (Section S8). The results confirmed that DBA should be the strongest binding site, with the MTA as the next preferred site, 6.8 kcal/mol higher. Binding of the macrocycle at TA1 and TA2 was, respectively, 14.5 and 15.6 kcal/mol higher than binding at the DBA site (Figure 2C). For molecular electronic devices, the perturbed highest occupied molecular orbitals (p-HOMOs) dominate carrier transport behavior because they correspond better to the Fermi level (0 eV) of the graphene electrodes than perturbed lowest occupied molecular orbitals (p-LOMOs). As the transmission peak

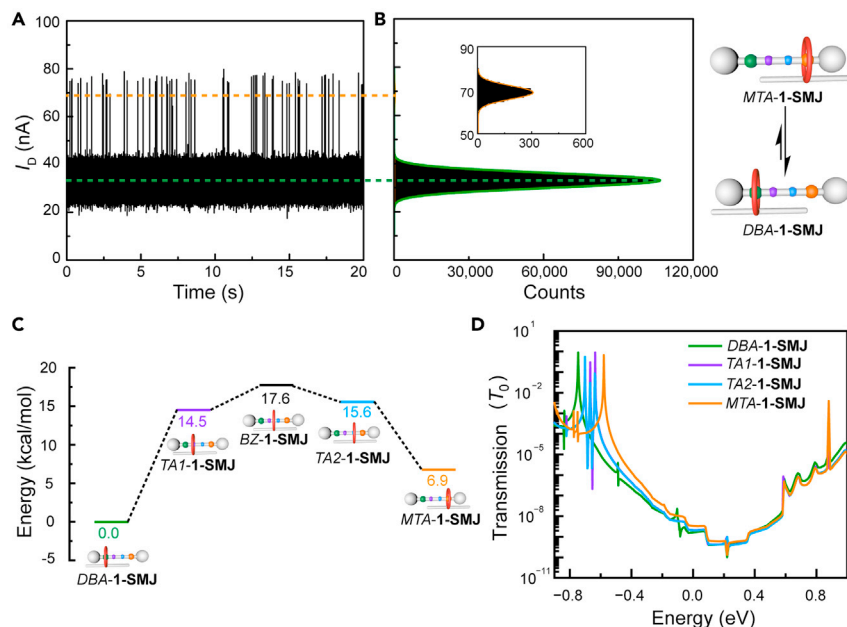


Figure 2. Real-time electrical characterization and computational analysis of 1-SMJ in CH₃CN at 298 K

(A) *I*-*t* curve of 1-SMJ immersed in CH₃CN at 298 K for 20 s with a sampling rate of 57.6 kSa/s. (B) The resulting current-count histogram from (A), showing a bimodal current distribution. The data, in combination with theoretical analysis, are consistent with the high state (orange) and low state (green) corresponding to the MTA-1-SMJ and DBA-1-SMJ co-conformers, respectively. (C) Simulated energy profile of the shuttling process of 1 in CH₃CN at 298 K. (D) Calculated transmission spectra of 1-SMJ in which the DB24C8 is located at the DBA (green), TA1 (purple), TA2 (blue), and MTA (orange) sites, respectively.

intensities of these four p-HOMOs are similar, the distance between the p-HOMOs and the electrode Fermi level (Figure 2D) determined that the increase of conductance with the sequence of DBA (−0.75 eV), TA1 ≈ TA2 (−0.64 eV), and MTA (−0.58 eV). Therefore, it is reasonable to relate the two distinct low and high current levels to the DBA-1-SMJ and MTA-1-SMJ co-conformers, respectively. The calculations not only shed light on the notable current differences observed during the measurements but also validate the relationship between the “low” and “high” states and shuttling of the macrocycle in 1-SMJ.

Temperature-dependent shuttling in acetonitrile

To investigate the effect of temperature on the shuttling process, the *I*-*t* curves of 1-SMJ devices immersed in acetonitrile (CH₃CN) were recorded at five different temperatures in the range of 288–328 K (Section S6.3) and the experiments were reproduced with a different set of 1-SMJs on a new device (Section S6.3). Similar current spikes and bimodal distributions were observed with faster conversion between the two states at higher temperatures. The resulting current-count distributions were always dominated by the low state, whereas the amount of the high state increased modestly with increasing temperature. Again, these observations are consistent with the rise in temperature resulting in a concomitant increase in the rate of shuttling of the DB24C8 macrocycle between the DBA and MTA binding sites. The increase in rates was also demonstrated for the collective behavior of 1 in CD₃CN solution: variable temperature ¹H NMR (VT-NMR) showed coalescence of signals for exchanging proton environments in the two co-conformers at 328 K (Section S7).

Table 1. Thermodynamic and kinetic parameters for the shuttling process between the DBA and MTA sites in 1-SMJ

Solvent	Temperature	$k_{DBA \rightarrow MTA}$ (s^{-1})	$k_{MTA \rightarrow DBA}$ (s^{-1})	$K_{MTA/DBA}$	$\Delta G_{MTA/DBA}^{\circ}$ (kcal/mol)	$\Delta H_{MTA/DBA}^{\circ}$ (kcal/mol)	$\Delta S_{MTA/DBA}^{\circ}$ (cal/mol·K)
CH ₃ CN	288 K	2.55 ± 0.33	$1.52 \pm 0.07 \times 10^3$	1.68×10^{-3}	3.64	6.09	8.55
	298 K	4.34 ± 0.10	$1.67 \pm 0.17 \times 10^3$	2.60×10^{-3}	3.51		
	308 K	6.61 ± 0.22	$1.89 \pm 0.14 \times 10^3$	3.50×10^{-3}	3.45		
	318 K	9.10 ± 1.49	$2.13 \pm 0.05 \times 10^3$	4.28×10^{-3}	3.43		
	328 K	16.68 ± 0.63	$2.50 \pm 0.13 \times 10^3$	6.67×10^{-3}	3.25		
DMSO	328 K	12.65 ± 0.25	$4.48 \pm 0.14 \times 10^2$	2.82×10^{-2}	2.32		

The kinetic analysis of the shuttling process was further refined by idealizing the *I*-*t* trajectories with Quantify Unknown Biophysics (QUB) software. One set of kinetic parameters (Table 1), including the average lifetime of each state (τ_{DBA} and τ_{MTA}), and the corresponding shuttling rate constant between two sites ($k_{DBA \rightarrow MTA}$ and $k_{MTA \rightarrow DBA}$, $k = 1/\tau$) were extracted from the single-exponential fittings of the dwell time (Figures 3A and 3B). The dwell time histograms indicated that most time intervals in the blocking events were subsecond, with both high- and low-state intervals fitting well to first-order decay exponentials, consistent with the shuttling between the two states being a first-order process in 1-SMJ. From 288 to 328 K the increase in shuttling rate with temperature for $k_{DBA \rightarrow MTA}$ ($\sim 6.5\times$) is higher than for $k_{MTA \rightarrow DBA}$ ($\sim 1.6\times$), reflecting a more significant temperature dependency of the binding affinity of the DBA site. The Arrhenius plot of temperature-dependent $\ln(k)$ in acetonitrile shows a linear relationship for $\ln(k)$ and $1,000/T$ from which activation energies of E_{DBA} (~ 8.39 kcal/mol) and E_{MTA} (~ 2.32 kcal/mol) for the shuttling processes in acetonitrile could be extracted (Figure 3C).

The equilibrium constant (K_a) is the ratio of the average lifetime of the two different states, which is equal to the ratio of the rate constants for forward and backward shuttling of the ring between the DBA and MTA sites. The resulting $K_{a(MTA/DBA)} = \tau_{MTA}/\tau_{DBA} = k_{DBA \rightarrow MTA}/k_{MTA \rightarrow DBA} = 2.60 \times 10^{-3}$ at 298 K indicates that the ring resides >99% of the time bound to the DBA group, reflecting the difference in binding affinities of DB24C8 for the two axle sites. This is in line with previously reported⁴⁸ bulk solution measurements of $K_{a(MTA/DAA)} = 2.5 \times 10^{-4}$ for a crown-ether-dialkylammonium(DAA)-MTA rotaxane in the less polar solvent, CH₂Cl₂. The increase in the $K_{a(MTA/DBA)}$ values for 1-SMJ with increasing temperature shows that the ring spends more time associated with the MTA site at higher temperatures. The Gibbs free energy ($\Delta G_{MTA/DBA}^{\circ}$) for the DBA to MTA shuttling process was determined from the K_a value, and the enthalpy ($\Delta H_{MTA/DBA}^{\circ}$) and entropy ($\Delta S_{MTA/DBA}^{\circ}$) obtained by linear fitting of the Van't Hoff equation [$-RT\ln(K_a) = \Delta H^{\circ} - T\Delta S^{\circ}$] (Figure 3D; Table 1).

Solvent-dependent shuttling measurements

Solvent can have a major influence on the operation of molecular machines (affecting both structure and dynamics), particularly with regard to solvation/desolvation effects and the polarity of the environment. The *I*-*t* curves for 1-SMJ in the highly polar solvent, dimethyl sulfoxide (DMSO), were recorded at 328 K to probe shuttling in that alternative medium. The results again showed what initially appeared to be a typical bimodal distribution, but more heavily skewed to a single major state (Figure 4A).

Statistical analysis (Section S6.4) shows that the $k_{MTA \rightarrow DBA}$ shuttling rate drops substantially (448.43 s⁻¹ (DMSO) versus $2,500.00$ s⁻¹ (CH₃CN)) compared with $k_{DBA \rightarrow MTA}$ (12.65 s⁻¹ (DMSO) versus 16.68 s⁻¹ (CH₃CN)). The $\Delta G_{MTA/DBA}^{\circ}$ also decreases ($\Delta G_{MTA/DBA}^{\circ} = 2.32$ (DMSO) versus 3.25 (CH₃CN) kcal/mol), whereas $K_{a(MTA/DBA)}$ increases ($K_{a(MTA/DBA)} = 2.82 \times 10^{-2}$ (DMSO) versus 6.67×10^{-3}

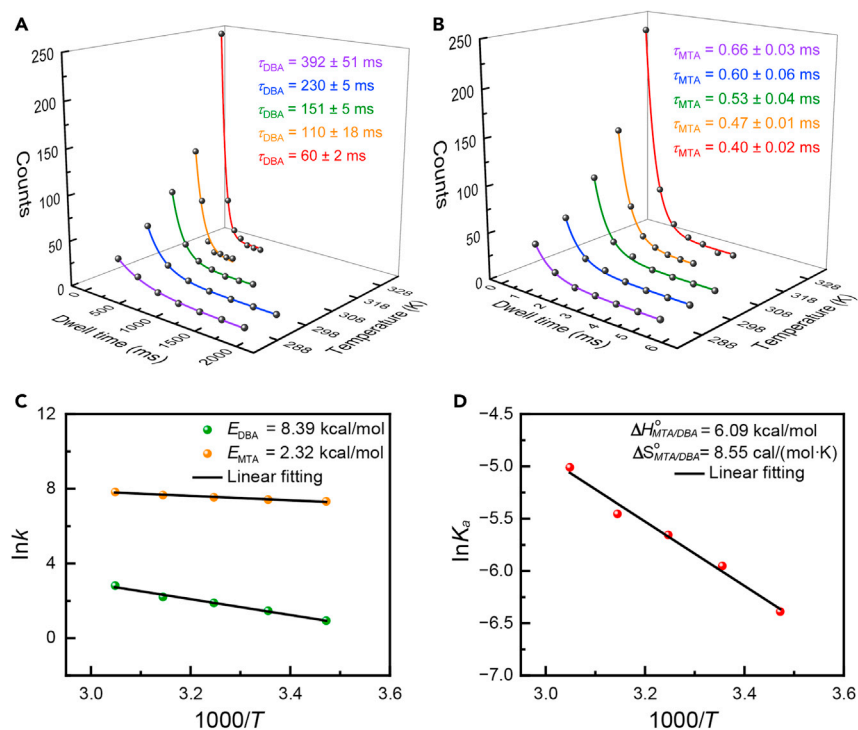


Figure 3. Thermodynamic and kinetic analysis of single-molecule shuttling dynamics in a 1-SMJ device at the graphene-acetonitrile interface

(A and B) Plots of the dwell times of the (A) DBA-1-SMJ and (B) MTA-1-SMJ current states and average state lifetimes (τ_{DBA} and τ_{MTA}) obtained from idealized fits in I - t trajectories obtained between 288 and 328 K.

(C) Arrhenius plots of activation energy of both sites ($E_{DBA} = 8.39$ kcal/mol, $E_{MTA} = 2.32$ kcal/mol).

(D) Plots of the thermodynamics parameters ($\ln K_a$ versus $1,000/T$). $\Delta G_{MTA/DBA}^\circ$ derived from $K_a(MTA/DBA)$ and $\Delta H_{MTA/DBA}^\circ$ and $\Delta S_{MTA/DBA}^\circ$ calculated using the Van't Hoff equation.

(CH₃CN)) (Table 1). The slower shuttling rate is somewhat surprising given that DMSO is a powerful hydrogen-bond-disrupting solvent, but it likely reflects the modest ability of DMSO to solvate the crown ether while the ring is displaced from the hydrogen-bonding sites of the axle. The difference in $\Delta G_{MTA/DBA}^\circ$ for 1-SMJ between the two solvents (0.93 kcal/mol) is broadly consistent with theoretical analysis (1.04 kcal/mol) (Figure 4B).

Observation of a weak-binding intermediate

At 338 K in DMSO, the existence of an additional infrequent, short-lived conducting state became noticeable during the transition between DBA-1-SMJ and MTA-1-SMJ. The average lifetime of the newly observable state is ~ 400 μ s (Figure 4C; Section S6.5). The state occurs reproducibly, typically appearing three or four times within a 20 s experiment. We attribute this intermediate with a very short dwell time to the TA1/TA2-1-SMJ states (Figure 2C). Accordingly, the shuttling process can now be pictured proceeding through three observable steps (Figure 4C): DB24C8 moving from the DBA site to the TA1/TA2 groups, and from there, either on to the MTA group or back to the original DBA site. The intermediate is stabilized by the formation of weak hydrogen bonds between the C-H of the triazole rings and the crown ether oxygen. As there are significant energy differences between DBA-1-SMJ and TA1/TA2-1-SMJ and between MTA-1-SMJ and TA1/TA2-1-SMJ under these conditions, only a few counts with a dwell time over the temporal resolution of the SMJ measurement (~ 17 μ s) could be captured

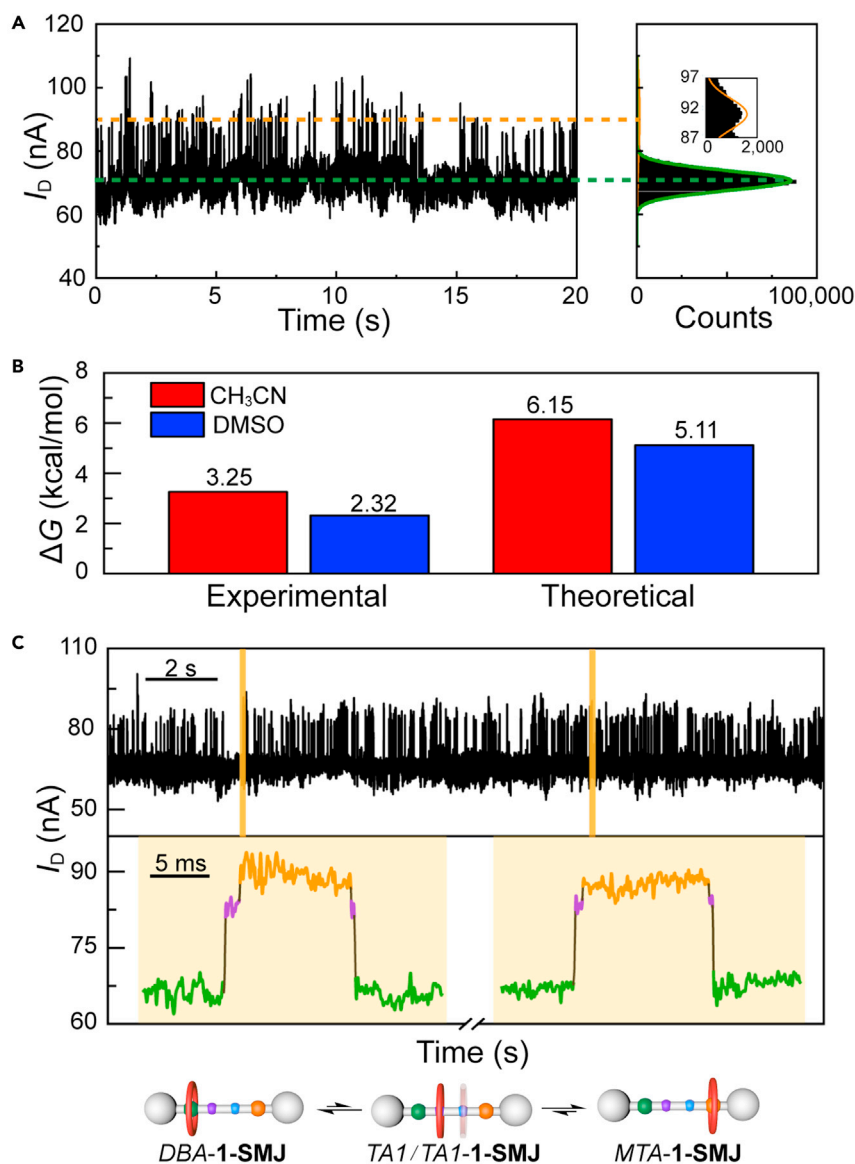


Figure 4. Real-time electrical characterization of 1-SMJ in DMSO and observation of a short-lived, weak-binding intermediate TA2/TA1-1-SMJ

(A) I - t curve and the resulting current-count histogram of 1-SMJ.

(B) Experimental and Calculated data of $\Delta G_{\text{MTA/DBA}}^{\ddagger}$ between CH_3CN and DMSO at 328 K.

(C) Partial I - t curve of 1-SMJ immersed in DMSO at 338 K for 20 s with a sampling rate of 57.6 kSa/s. The expanded region of the I - t curve (yellow region) shows a noticeable conducting state (labeled in purple) existing during the transition of the macrocycle between the DBA (labeled in green) and MTA (labeled in orange) sites with an average lifetime of 400 μs . This intermediate is likely to be the TA1/TA2-1-SMJ co-conformers. The shuttling process from DBA to-and-from MTA via this short-lived intermediate state is pictured in three steps.

across the 20 s measuring time. The limited amount of data for these events precluded the extraction of kinetic and thermodynamic parameters. The scarcity of the intermediate state also means that it contributes little to a time-average structure; therefore, it is not apparent using techniques, such as NMR spectroscopy. This illustrates the value of the individual molecule interrogation possible with GMG-SMJs and complementary techniques, such as AFM and optical tweezers. The

GMG-SMJs provide sufficient structural (~ 1 nm) and temporal resolution (~ 17 μ s) to reveal the stepwise stochastic dynamics of ring movement that occurs over 4 nm in a single molecular shuttle. Understanding how the composition of components influences machine dynamics should be useful for informing the design of future artificial molecular machines.

EXPERIMENTAL PROCEDURES

Resource availability

Lead contact

Liang Zhang, zhangliang@chem.ecnu.edu.cn

David A. Leigh, david.leigh@manchester.ac.uk

Xuefeng Guo, guoxf@pku.edu.cn

Materials availability

This study did not generate new reagents.

Data and code availability

Conductance data from the GMG-SMJ measurements is available on request from X.G.

SUPPLEMENTAL INFORMATION

Supplemental information can be found online at <https://doi.org/10.1016/j.chempr.2021.11.012>.

ACKNOWLEDGMENTS

L.Z. and D.A.L. thank East China Normal University for funding. L.Z. thanks the National Natural Science Foundation of China (22001074) and the Shanghai Sailing Program (20YF1411400) for funding. S.C. thanks the Postdoctoral Research Foundation of China (2019M661432) for funding. D.S. and X.G. thank the National Key R&D Program of China (2017YFA0204901), the National Natural Science Foundation of China (21727806 and 21933001), the Tencent Foundation through the XPLOER PRIZE and Frontiers Science Center for New Organic Matter at Nankai University (63181206) for funding. Y.L. thanks Shenzhen Fundamental Research Program (JCYJ20190807094003691) for funding. D.A.L. is a Royal Society Research Professor.

AUTHOR CONTRIBUTIONS

L.Z. planned the work. S.C. performed the synthesis and D.S. carried out the single-molecule junction measurement. S.C. and D.S. contributed equally to this work. Y.L. and X.L. performed the simulations. L.Z., D.A.L., C.J., and X.G. directed the research. All authors contributed to the data analysis and the writing of the manuscript.

DECLARATION OF INTERESTS

The authors declare no competing interests.

Received: September 3, 2021

Revised: October 7, 2021

Accepted: November 9, 2021

Published: December 3, 2021

REFERENCES

1. Bruns, C.J., and Stoddart, J.F. (2016). The fundamentals of making mechanical bonds. In *The Nature of the Mechanical Bond: From Molecules to Machines* (Wiley), pp. 55–268.
2. Sauvage, J.-P. (2017). From chemical topology to molecular machines (Nobel lecture). *Angew. Chem. Int. Ed. Engl.* **56**, 11080–11093. <https://doi.org/10.1002/anie.201702992>.
3. Stoddart, J.F. (2017). Mechanically interlocked molecules (MIMs)—molecular shuttles, switches, and machines (Nobel lecture). *Angew. Chem. Int. Ed. Engl.* **56**, 11094–11125. <https://doi.org/10.1002/anie.201703216>.
4. Kay, E.R., Leigh, D.A., and Zerbetto, F. (2007). Synthetic molecular motors and mechanical machines. *Angew. Chem. Int. Ed. Engl.* **46**, 72–191. <https://doi.org/10.1002/anie.200504313>.
5. Erbas-Cakmak, S., Leigh, D.A., McTernan, C.T., and Nussbaumer, A.L. (2015). Artificial molecular machines. *Chem. Rev.* **115**, 10081–10206. <https://doi.org/10.1021/acs.chemrev.5b00146>.
6. Zhang, L., Marcos, V., and Leigh, D.A. (2018). Molecular machines with bio-inspired mechanisms. *Proc. Natl. Acad. Sci. USA* **115**, 9397–9404. <https://doi.org/10.1073/pnas.1712788115>.
7. Evans, N.H. (2019). Recent advances in the synthesis and application of hydrogen bond templated rotaxanes and catenanes. *Eur. J. Org. Chem.* **2019**, 3320–3343. <https://doi.org/10.1002/ejoc.201900081>.
8. Sluysmans, D., and Stoddart, J.F. (2019). The burgeoning of mechanically interlocked molecules in chemistry. *Trends in Chemistry* **1**, 185–197. <https://doi.org/10.1016/j.trechm.2019.02.013>.
9. Panman, M.R., Bodis, P., Shaw, D.J., Bakker, B.H., Newton, A.C., Kay, E.R., Brouwer, A.M., Buma, W.J., Leigh, D.A., and Woutersen, S. (2010). Operation mechanism of a molecular machine revealed using time-resolved vibrational spectroscopy. *Science* **328**, 1255–1258. <https://doi.org/10.1126/science.1187967>.
10. Rijs, A.M., Sändig, N., Blom, M.N., Oomens, J., Hannam, J.S., Leigh, D.A., Zerbetto, F., and Buma, W.J. (2010). Controlled hydrogen-bond breaking in a rotaxane by discrete solvation. *Angew. Chem. Int. Ed. Engl.* **49**, 3896–3900. <https://doi.org/10.1002/anie.201001231>.
11. Ragazzon, G., Credi, A., and Colasson, B. (2017). Thermodynamic insights on a bistable acid–base switchable molecular shuttle with strongly shifted co-conformational equilibria. *Chem. Eur. J.* **23**, 2149–2156. <https://doi.org/10.1002/chem.201604783>.
12. Kumpulainen, T., Panman, M.R., Bakker, B.H., Hilbers, M., Woutersen, S., and Brouwer, A.M. (2019). Accelerating the shuttling in hydrogen-bonded rotaxanes: active role of the axle and the end station. *J. Am. Chem. Soc.* **141**, 19118–19129. <https://doi.org/10.1021/jacs.9b10005>.
13. Scarel, F., Valenti, G., Gaikwad, S., Marcaccio, M., Paolucci, F., and Mateo-Alonso, A. (2012). A molecular shuttle driven by fullerene radical-anion recognition. *Chem. Eur. J.* **18**, 14063–14068. <https://doi.org/10.1002/chem.201201264>.
14. Young, P.G., Hirose, K., and Tobe, Y. (2014). Axle length does not affect switching dynamics in degenerate molecular shuttles with rigid spacers. *J. Am. Chem. Soc.* **136**, 7899–7906.
15. Gholami, G., Zhu, K., Baggi, G., Schott, E., Zarate, X., and Loeb, S.J. (2017). Influence of axle length on the rate and mechanism of shuttling in rigid H-shaped [2]rotaxanes. *Chem. Sci.* **8**, 7718–7723. <https://doi.org/10.1039/c7sc03736h>.
16. Zhu, K., Baggi, G., and Loeb, S.J. (2018). Ring-through-ring molecular shuttling in a saturated [3]rotaxane. *Nat. Chem.* **10**, 625–630.
17. A.-S. Duwez, and N. Willet, eds. (2011). *Molecular Manipulation with Atomic Force Microscopy* (CRC Press).
18. Clausen-Schaumann, H., Seitz, M., Krautbauer, R., and Gaub, H.E. (2000). Force spectroscopy with single bio-molecules. *Curr. Opin. Chem. Biol.* **4**, 524–530. [https://doi.org/10.1016/S1367-5931\(00\)00126-5](https://doi.org/10.1016/S1367-5931(00)00126-5).
19. Brough, B., Northrop, B.H., Schmidt, J.J., Tseng, H.R., Houk, K.N., Stoddart, J.F., and Ho, C.M. (2006). Evaluation of synthetic linear motor-molecule actuation energetics. *Proc. Natl. Acad. Sci. USA* **103**, 8583–8588. <https://doi.org/10.1073/pnas.0509645103>.
20. Lussis, P., Svaldo-Lanero, T., Bertocco, A., Fustin, C.-A., Leigh, D.A., and Duwez, A.-S. (2011). A single synthetic small molecule that generates force against a load. *Nat. Nanotechnol.* **6**, 553–557. <https://doi.org/10.1038/nnano.2011.132>.
21. Sluysmans, D., Lussis, P., Fustin, C.A., Bertocco, A., Leigh, D.A., and Duwez, A.-S. (2021). Real-time fluctuations in single-molecule rotaxane experiments reveal an intermediate weak binding state during shuttling. *J. Am. Chem. Soc.* **143**, 2348–2352. <https://doi.org/10.1021/jacs.0c12161>.
22. Van Quaethem, A., Lussis, P., Leigh, D.A., Duwez, A.-S., and Fustin, C.-A. (2014). Probing the mobility of catenane rings in single molecules. *Chem. Sci.* **5**, 1449–1452. <https://doi.org/10.1039/C3SC53113A>.
23. Sluysmans, D., Hubert, S., Bruns, C.J., Zhu, Z., Stoddart, J.F., and Duwez, A.S. (2018). Synthetic oligorotaxanes exert high forces when folding under mechanical load. *Nat. Nanotechnol.* **13**, 209–213. <https://doi.org/10.1038/s41565-017-0033-7>.
24. Sluysmans, D., Devaux, F., Bruns, C.J., Stoddart, J.F., and Duwez, A.-S. (2018). Dynamic force spectroscopy of synthetic oligorotaxane foldamers. *Proc. Natl. Acad. Sci. USA* **115**, 9362–9366. <https://doi.org/10.1073/pnas.1712790115>.
25. Naranjo, T., Lemishko, K.M., de Lorenzo, S., Somoza, Á., Ritort, F., Pérez, E.M., and Ibarra, B. (2018). Dynamics of individual molecular shuttles under mechanical force. *Nat. Commun.* **9**, 4512. <https://doi.org/10.1038/s41467-018-06905-8>.
26. Xin, N., Guan, J., Zhou, C., Chen, X., Gu, C., Li, Y., Ratner, M.A., Nitzan, A., Stoddart, J.F., and Guo, X. (2019). Concepts in the design and engineering of single-molecule electronic devices. *Nat. Rev. Phys.* **1**, 211–230. <https://doi.org/10.1038/s42254-019-0022-x>.
27. Wen, H., Li, W., Chen, J., He, G., Li, L., Olson, M.A., Sue, A.C.-H., Stoddart, J.F., and Guo, X. (2016). Complex formation dynamics in a single-molecule electronic device. *Sci. Adv.* **2**, e1601113. <https://doi.org/10.1126/sciadv.1601113>.
28. Liu, Z., Li, X., Masai, H., Huang, X., Tsuda, S., Terao, J., Yang, J., and Guo, X. (2021). A single-molecule electrical approach for amino acid detection and chirality recognition. *Sci. Adv.* **7**, eabe4365. <https://doi.org/10.1126/sciadv.abe4365>.
29. Zhou, C., Li, X., Masai, H., Liu, Z., Lin, Y., Tamaki, T., Terao, J., Yang, J., and Guo, X. (2019). Revealing charge- and temperature-dependent movement dynamics and mechanism of individual molecular machines. *Small Methods* **3**, 1900464. <https://doi.org/10.1002/smt.201900464>.
30. Guan, J., Jia, C., Li, Y., Liu, Z., Wang, J., Yang, Z., Gu, C., Su, D., Houk, K.N., Zhang, D., and Guo, X. (2018). Direct single-molecule dynamic detection of chemical reactions. *Sci. Adv.* **4**, eaar2177. <https://doi.org/10.1126/sciadv.aar2177>.
31. Gu, C., Hu, C., Wei, Y., Lin, D., Jia, C., Li, M., et al. (2018). Label-free dynamic detection of single-molecule nucleophilic-substitution reactions. *Nano Lett.* **18**, 4156–4162. <https://doi.org/10.1021/acs.nanolett.8b00949>.
32. Yang, C., Liu, Z., Li, Y., Zhou, S., Lu, C., Guo, Y., Ramirez, M., Zhang, Q., Li, Y., Liu, Z., et al. (2021). Electric field-catalyzed single-molecule Diels-Alder reaction dynamics. *Sci. Adv.* **7**, eabf0689. <https://doi.org/10.1126/sciadv.abf0689>.
33. Yang, C., Zhang, L., Lu, C., Zhou, S., Li, X., Li, Y., et al. (2021). Unveiling the full reaction path of the Suzuki-Miyaura cross-coupling in a single-molecule junction. *Nat. Nanotechnol.* **16**, 1214–1223. <https://doi.org/10.1038/s41565-021-00959-4>.
34. Zhou, C., Li, X., Gong, Z., Jia, C., Lin, Y., Gu, C., He, G., Zhong, Y., Yang, J., and Guo, X. (2018). Direct observation of single-molecule hydrogen-bond dynamics with single-bond resolution. *Nat. Commun.* **9**, 807. <https://doi.org/10.1038/s41467-018-03203-1>.
35. Green, J.E., Choi, J.W., Boukai, A., Bunimovich, Y., Johnston-Halperin, E., Delonno, E., et al. (2007). A 160-kilobit molecular electronic memory patterned at 10¹¹ bits per square centimetre. *Nature* **445**, 414–417. <https://doi.org/10.1038/nature05462>.
36. Chen, H., and Fraser Stoddart, J.F. (2021). From molecular to supramolecular electronics. *Nat. Rev. Mater.* **6**, 804–828. <https://doi.org/10.1038/s41578-021-00302-2>.
37. Coutrot, F., and Busseron, E. (2008). A new glycorotaxane molecular machine based on an anilinium and a triazolium station. *Chem. Eur. J.*

- 14, 4784–4787. <https://doi.org/10.1002/chem.200800480>.
38. Coutrot, F., Romuald, C., and Busseron, E. (2008). A new pH-switchable dimannosyl [c2] daisy chain molecular machine. *Org. Lett.* 10, 3741–3744. <https://doi.org/10.1021/ol801390h>.
39. Busseron, E., Romuald, C., and Coutrot, F. (2010). Bistable or oscillating state depending on station and temperature in three-station glycorotaxane molecular machines. *Chem. Eur. J.* 16, 10062–10073. <https://doi.org/10.1002/chem.201000777>.
40. Jiang, Y., Guo, J.B., and Chen, C.F. (2010). A new [3]rotaxane molecular machine based on a dibenzylammonium ion and a triazolium station. *Org. Lett.* 12, 4248–4251. <https://doi.org/10.1021/ol101920b>.
41. Jiang, Q., Zhang, H.Y., Han, M., Ding, Z.J., and Liu, Y. (2010). pH-Controlled intramolecular charge-transfer behavior in bistable [3] rotaxane. *Org. Lett.* 12, 1728–1731. <https://doi.org/10.1021/ol100321k>.
42. Blanco, V., Carlone, A., Hänni, K.D., Leigh, D.A., and Lewandowski, B. (2012). A rotaxane-based switchable organocatalyst. *Angew. Chem. Int. Ed. Engl.* 51, 5166–5169. <https://doi.org/10.1002/anie.201201364>.
43. Erbas-Cakmak, S., Fielden, S.D.P., Karaca, U., Leigh, D.A., McTernan, C.T., Tetlow, D.J., and Wilson, M.R. (2017). Rotary and linear molecular motors driven by pulses of a chemical fuel. *Science* 358, 340–343. <https://doi.org/10.1126/science.aao1377>.
44. Blanco, V., Leigh, D.A., Marcos, V., Morales-Serna, J.A., and Nussbaumer, A.L. (2014). A switchable [2]rotaxane asymmetric organocatalyst that utilizes an acyclic chiral secondary amine. *J. Am. Chem. Soc.* 136, 4905–4908. <https://doi.org/10.1021/ja501561c>.
45. Ragazzon, G., Baroncini, M., Silvi, S., Venturi, M., and Credi, A. (2015). Light-powered autonomous and directional molecular motion of a dissipative self-assembling system. *Nat. Nanotechnol.* 10, 70–75. <https://doi.org/10.1038/nnano.2014.260>.
46. Canton, M., Groppi, J., Casimiro, L., Corra, S., Baroncini, M., Silvi, S., and Credi, A. (2021). Second-generation light-fueled supramolecular pump. *J. Am. Chem. Soc.* 143, 10890–10894. <https://doi.org/10.1021/jacs.1c06027>.
47. Groppi, J., Casimiro, L., Canton, M., Corra, S., Jafari-Nasab, M., Tabacchi, G., Cavallo, L., Baroncini, M., Silvi, S., Fois, E., and Credi, A. (2020). Precision molecular threading/dethreading. *Angew. Chem. Int. Ed. Engl.* 59, 14825–14834. <https://doi.org/10.1002/anie.202003064>.
48. Colasson, B., Credi, A., and Ventura, B. (2020). Photoinduced electron transfer involving a naphthalimide chromophore in switchable and flexible [2]rotaxanes. *Chem. Eur. J.* 26, 534–542. <https://doi.org/10.1002/chem.201904155>.